

Nonparametric Kernel Density Estimation Near the Boundary

Peter Malec^{a,*}, Melanie Schienle^b

^a*Institute for Statistics and Econometrics, Humboldt-Universität zu Berlin,
Spandauer Str. 1, D-10178 Berlin, Germany.*

^b*Institute for Empirical Economics, Leibniz University Hannover,
Königswoerther Platz 1, D-30167 Hannover, Germany.*

Abstract

Standard fixed symmetric kernel type density estimators are known to encounter problems for positive random variables with a large probability mass close to zero. It is shown that, in such settings, alternatives of asymmetric gamma kernel estimators are superior, but also differ in asymptotic and finite sample performance conditional on the shape of the density near zero and the exact form of the chosen kernel. Therefore, a refined version of the gamma kernel with an additional tuning parameter according to the shape of the density close to the boundary is suggested. A data-driven method for the appropriate choice of the modified gamma kernel estimator is also provided. An extensive simulation study compares the performance of this refined estimator to standard gamma kernel estimates and standard boundary corrected and adjusted fixed kernels. It is found that the finite sample performance of the proposed new estimator is superior in all settings. Two empirical applications based on high-frequency stock trading volumes and realized volatility forecasts demonstrate the usefulness of the proposed methodology in practice.

Keywords: kernel density estimation, boundary correction, asymmetric kernel

*Corresponding author. Address: Institute for Statistics and Econometrics, Humboldt-Universität zu Berlin, Spandauer Str. 1, D-10178 Berlin, Germany. Email: malecpet@hu-berlin.de. Phone: +49-(0)30-2093-5725. Fax: +49-(0)30-2093-5712.

Email addresses: malecpet@hu-berlin.de (Peter Malec),
schienle@ewifo.uni-hannover.de (Melanie Schienle)

1. Introduction

There are many applications in particular in economics where densities of positive random variables are the object of interest or an essential model ingredient to be estimated from data. Compare, e.g., income data, financial transaction data, volatility models, but also duration and survival times data. In a lot of these situations, however, appropriate functional forms are unknown or controversial, such that a nonparametric estimate is needed. It is often the point estimates close to the boundary which are in the focus of practical interest and thus, require good precision.

For cases of densities where most of the data is concentrated away from the boundary, there is a huge literature on boundary correction techniques of the standard symmetric fixed kernel density estimator. Such adjustments are needed at points close to the boundary, since fixed kernels might assign positive weight outside the support yielding inconsistent results. Among these techniques count e.g. the cut- and normalized kernel (see Gasser and Müller, 1979), the reflection method (see Schuster, 1958) and the generalized reflection estimator (see Karunamuni and Alberts, 2005).

If, however, the true density might have substantial mass close to the boundary, there are superior methods, such as the boundary kernel of Jones (1993). As this estimator could yield negative point estimates, this is corrected by Jones and Foster (1996) at some minor cost of performance (see Jones, 1993). In comparison, the combination of polynomial transformation followed by reflection as in Marron and Ruppert (1994) is much less flexible, working well exclusively at boundaries if the initial transformation is close enough to the density shape near zero.

Nonparametric kernel density estimators with asymmetric kernels, such as gamma kernels, have been introduced to improve upon the performance of fixed kernels at the boundary. In particular for positive random variables, their flexible shape avoids the boundary consistency problem and directly yields positive estimates by construction (see Chen, 2000). Moreover, in this class of nonnegative kernel density estimators, asymmetric kernels achieve the optimal rate of convergence in the sense of the mean integrated squared error (MISE) (see, e.g., Scaillet, 2004; Chen, 2000). Furthermore, their variance decreases the further points of estimation move away from the boundary. This leads to an advantage in situations of naturally unbalanced scattered design points in particular for densities with sparse areas (see, e.g., Chen, 1999; Michels, 1992; Haggmann and Scaillet, 2007). As generally boundary

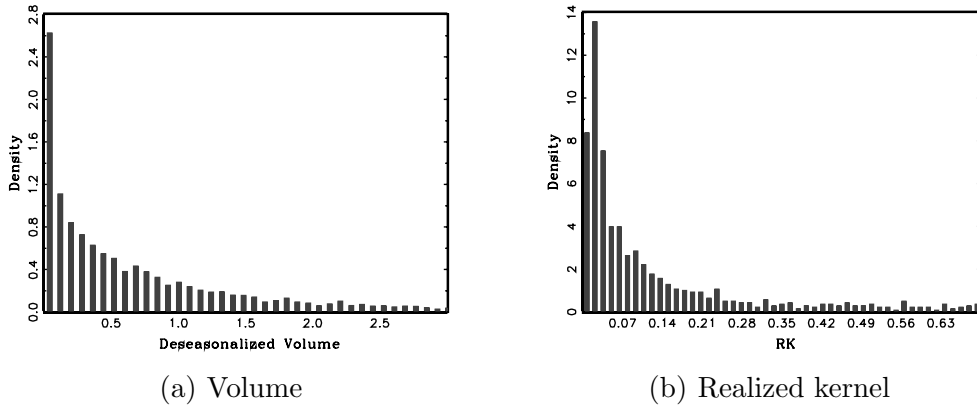


Figure 1: Histograms of intraday trading volumes and realized kernel estimates. We consider deseasonalized nonzero 15-Second trading volumes of Citigroup and realized kernel estimates for JP Morgan. Sample period: February 2009 (trading volumes), January 2006 – December 2009 (realized kernel). For details on the seasonal adjustment of trading volumes and computation of the realized kernel, see Section 4.

and unequal design issues get increasingly severe for higher dimensions, the use of gamma kernels especially pays off for multivariate density or regression problems (see Bouezmarni and Rombouts, 2010a). We also demonstrate this in a simple multivariate setup as part of our simulation study. The effect becomes very pronounced and therefore of particular relevance for the extreme case of functional data analysis (see Ferraty and Vieu, 2006; Quintela del Ro et al., 2011; Ferraty et al., 2012).

We contribute to the extensive literature on kernel estimation near the boundary by clearly identifying design situations in which finite sample and asymptotic performance of gamma kernel estimates are distinctly superior to any competing fixed kernel adjusted estimates and thus, should be strictly preferred. Such situations occur when the true f approaches the boundary with a derivative f' significantly different from zero. Such density shapes naturally appear in high-frequency data, e.g., when studying aggregated trading volumes (see Figure 1), but also in many other applications, such as spectral density estimation of long memory time series or when modeling volatilities in particular on the intra-daily level (see, e.g., Robinson and Henry, 2003; Corradi et al., 2009).

But we also show that, depending on the underlying shape of the true density, the two existing gamma kernel estimators, the so-called standard

and modified version as introduced in Chen (2000), might differ substantially in boundary performance and still leave significant room for improvement. While in practice almost exclusively a modified gamma-type kernel estimator is used, we find that, in particular for pole situations, the standard gamma-type estimator yields large performance advantages. We therefore introduce a simple data-driven criterion identifying such extreme settings.

For all other design situations, we propose a refined gamma kernel estimator, which outperforms all existing estimators in a comprehensive finite sample study. The new estimator introduces a modification parameter according to the shape of f and its first two derivatives close to the boundary. For determining the appropriate specification of this refined gamma kernel estimator in practice, we also provide an automatic procedure.

Our two applications clearly demonstrate the significant impact of a design dependent choice of gamma-type kernels on the overall estimation results. For high-frequency stock trading volumes, we detect a pole situation and obtain an improved fit from the standard gamma kernel estimator as opposed to the generally applied modified one. In realized variance forecasts, the new refined gamma kernel estimator is the only one which yields results consistent with financial theory, while all other competing estimators produce an unexpected bias.

2. Kernel Density Estimation at the Boundary

Throughout the paper, we study density estimation for the case that the support $S_X \subset \mathbb{R}$ of an unknown density is bounded from one side. Without loss of generality, we take this bound to be a lower bound and equal to zero as in many applications like wage distributions, distributions of trading volumes, etc. Obtained results, however, can be easily generalized by appropriate translations and reflections at the y-axis. Note also that we restrict our initial theoretical exposition to the case of univariate densities for ease of notation. Multivariate extensions are then systematically straightforward via product kernels. We illustrate this in a simple simulation exercise in a multivariate setting in Section 3, which highlights the gains from using our method in particular for higher dimensions.

For a random sample $\{X_i\}_{i=1}^n$ from a distribution with unknown density

$f_X(x)$, the conventional kernel density estimator has the form

$$\hat{f}_X(x) = \frac{1}{nb} \sum_{i=1}^n K\left(\frac{x - X_i}{b}\right), \quad (1)$$

where b is a smoothing bandwidth with $b \rightarrow 0$ and $nb \rightarrow \infty$ as $n \rightarrow \infty$, while K is a kernel function which integrates to unity, i.e. $\int K(u) du = 1$. If the shape of K is symmetric and fixed across the support, estimation and inference are generally simplified for unbounded support. But if zero bounds the support S_X from below, \hat{f}_X is inconsistent at the boundary $[0, b)$ for such simplistic choices of K . The literature has therefore provided many suggestions for adjustments in fixed kernel estimation, which we will outline in more detail when they appear as benchmarks in the simulation study in Section 3. What characterizes all these approaches, however, is that they mostly work well only for specific forms of f_X in the boundary region and/or can yield negative estimates. In particular, for densities with non-vanishing probability mass close to zero as in Figure 1, these standard correction methods perform poorly at the boundary. In applications, it is exactly this boundary region which is in the focus of attention and requires precise estimates.

2.1. Standard Asymmetric Kernel Density Estimators

Density estimators based on kernels of locally varying form have been shown to exhibit a good performance for a wide range of shapes of the underlying true density. Such kernels are nonnegative, but no longer symmetric, adjusting in skewness along the support. For the considered one-sided boundary problem, gamma kernel estimators are the simplest and most popular forms of such flexible estimators. In case of a two-sided boundary, which is not our focus here, beta kernels would be the appropriate choice (see Chen, 1999). There are two alternative specifications of gamma kernel estimators proposed by Chen (2000), of which the first kind is defined as

$$\hat{f}_X^\gamma(x) = \frac{1}{n} \sum_{i=1}^n K_{x/b+1,b}^\gamma(X_i), \quad (2)$$

where $K_{x/b+1,b}^\gamma$ denotes the density of the gamma distribution with shape parameter $x/b + 1$ and scale parameter b , i.e.

$$K_{x/b+1,b}^\gamma(u) = \frac{u^{x/b} \exp(-u/b)}{b^{x/b+1} \Gamma(x/b + 1)}. \quad (3)$$

Consistency and asymptotic normality of the above estimator are straightforward to derive under standard assumptions. See, e.g., Chen (2000) for the pointwise and Hagmann and Scaillet (2007) for the uniform version. For time series observations, consistency can also be obtained under mixing assumptions as in Bouezmarni and Rombouts (2010b). In particular, for a sufficiently smooth density $f_X \in C^2(S_X)$, it can be shown that bias and variance vanish asymptotically for $b \rightarrow 0$ and $nb \rightarrow \infty$. Their asymptotic forms are

$$\text{Bias}\left\{\hat{f}_X^\gamma(x)\right\} = b \left\{f'_X(x) + \frac{1}{2}x f''_X(x)\right\} + o(b), \quad (4)$$

and

$$\text{Var}\left\{\hat{f}_X^\gamma(x)\right\} \approx \begin{cases} \frac{f_X(x)}{nb} \mathcal{C}_b(x) & \text{if } x/b \rightarrow \kappa, \\ \frac{f_X(x)}{2\sqrt{\pi}} (xb)^{-1/2} n^{-1} & \text{if } x/b \rightarrow \infty, \end{cases} \quad (5)$$

where κ is a nonnegative constant and $\mathcal{C}_b(x) = \frac{\Gamma(2\kappa+1)}{2^{1+2\kappa} \Gamma^2(\kappa+1)}$. Accordingly, the asymptotic mean squared error is

$$\text{MSE}\left\{\hat{f}_X^\gamma(x)\right\} \approx \begin{cases} b^2 \left\{f'_X(x) + \frac{1}{2}x f''_X(x)\right\}^2 + \frac{f_X(x)}{nb} \mathcal{C}_b(x) & \text{if } x/b \rightarrow \kappa, \\ b^2 \left\{f'_X(x) + \frac{1}{2}x f''_X(x)\right\}^2 + \frac{f_X(x)}{2n\sqrt{\pi}} (xb)^{-1/2} & \text{if } x/b \rightarrow \infty. \end{cases} \quad (6)$$

Note that the asymptotic variance decreases for large x , which is offset by an increasing bias. In contrast to fixed kernel estimators, the asymptotic bias contains the first derivative of the density f'_X , which is due to the fact that the chosen flexible kernel shape has its mode rather than its mean at the point of estimation x . The modified gamma kernel estimator improves on this for most of the support without generating convergence problems in the boundary region. In particular, it uses the pdf of a gamma distribution with shape parameter x/b and scale parameter b as kernel function in the interior

of the support. This distribution has mean x , but is unbounded for x approaching zero. Therefore, the kernel function consists of two regimes, where the boundary form is chosen ad hoc, ensuring a smooth connection to the desired interior shape, while avoiding unboundedness problems. According to Chen (2000), the estimator is thus defined as

$$\hat{f}_X^{\gamma m}(x) = \frac{1}{n} \sum_{i=1}^n K_{\rho_b(x), b}^{\gamma}(X_i), \quad (7)$$

where

$$\rho_b(x) = \begin{cases} \frac{1}{4} \left(\frac{x}{b}\right)^2 + 1 & \text{if } x \in [0, 2b), \\ x/b & \text{if } x \in [2b, \infty). \end{cases} \quad (8)$$

Note that the estimator fixes the size of the boundary region to the area from 0 to $2b$ independent of the shape of the underlying true density. The asymptotic bias of the modified gamma kernel estimator has the desired leading term

$$\text{Bias}\left\{\hat{f}_X^{\gamma m}(x)\right\} = \begin{cases} \xi_b(x) b f_X'(x) + o(b) & \text{if } x \in [0, 2b), \\ \frac{1}{2} x f_X''(x) b + o(b) & \text{if } x \in [2b, \infty), \end{cases} \quad (9)$$

where $\xi_b(x) = (1-x) \{\rho_b(x) - x/b\} / \{1 + b\rho_b(x) - x\}$, which is in $[0, 1]$ given standard choices of $b < 0.5$ for all $x \in [0, 2b)$ (see Figure 2). Its variance can be shown to have the same structure as in (5) with modified constant $\tilde{\mathcal{C}}_b(x) = \frac{\Gamma(2\kappa^2+1)}{2^{1+2\kappa^2}\Gamma^2(\kappa^2+1)}$ and

$$\text{MSE}\left\{\hat{f}_X^{\gamma m}(x)\right\} \approx \begin{cases} \left\{\xi_b(x) b f_X'(x)\right\}^2 + \frac{f_X(x)}{nb} \tilde{\mathcal{C}}_b(x) & \text{if } x/b \rightarrow \kappa, \\ \left\{\frac{1}{2} x f_X''(x) b\right\}^2 + \frac{f_X(x)}{2n\sqrt{\pi}} (xb)^{-1/2} & \text{if } x/b \rightarrow \infty. \end{cases} \quad (10)$$

See Chen (2000) for details on the derivations.

2.2. Choice of Estimators for Different Density Shapes Near Zero

In general in the literature, the modified gamma kernel estimator has been strictly preferred over the standard gamma kernel version. Although a simple comparison of their asymptotic variances reveals that the constant for the modified estimator, $\tilde{\mathcal{C}}_b$, is strictly larger than its counterpart for the standard

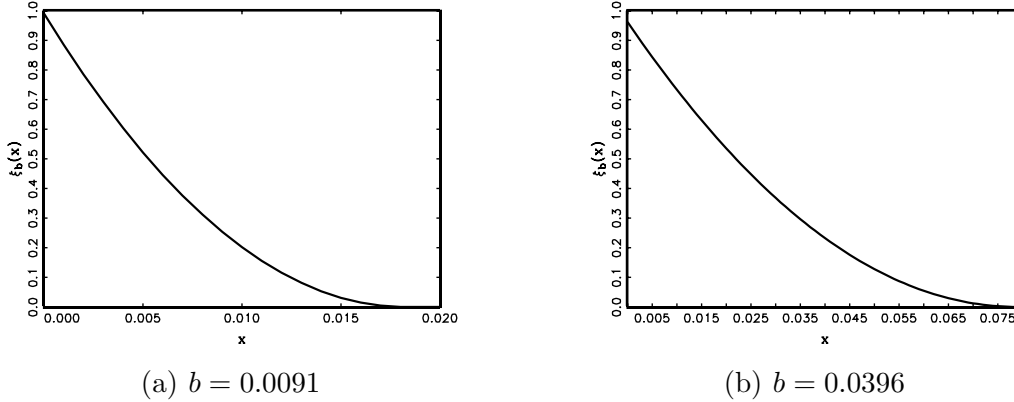


Figure 2: $\xi_b(x)$. Scale factor $\xi_b(x) = (1 - x) \{\rho_b(x) - x/b\} / \{1 + b\rho_b(x) - x\}$ entering asymptotic bias and variance of the modified gamma kernel estimator. Bandwidths of two DGPs from the simulation study in Section 3 are used.

gamma kernel, \mathcal{C}_b , close to the boundary (for all $\kappa < 1$), the above choice has been justified by the similarity of the modified gamma kernel to fixed kernels in terms of asymptotic bias behavior as displayed in (9). However, when carefully comparing the leading asymptotic bias terms of both gamma-type estimators, we find that there are cases where it is asymptotically favorable to use the standard gamma kernel estimator. For all $x > 2b$, in the interior of the support with

$$|0.5x f_X''(x)| > |f_X'(x) + 0.5x f_X''(x)|, \quad (11)$$

the standard gamma kernel should be preferred over the modified version. This occurs, in particular, for areas where the density satisfies the shape restrictions

$$0 < -f_X'(x)/f_X''(x) < x. \quad (12)$$

The lower bound is fulfilled for values x where f_X' and f_X'' have different signs, i.e. where the density f_X is either decreasing and convex or where it is concave and increasing. In the first case, it can be shown that if f_X has a pole at zero, then trivially also the upper bound of (12) is satisfied. If additionally f_X does not have any local maxima, the standard gamma kernel should be preferred over the modified version for the entire interior support (see Figure 3). Our simulation study below confirms that this is also of

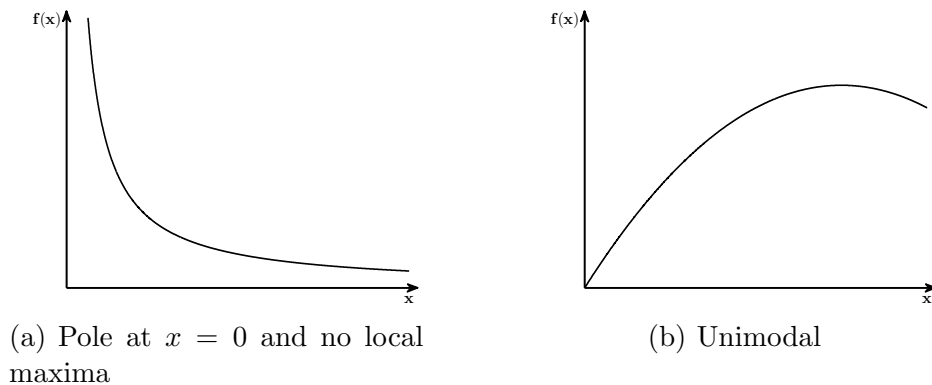


Figure 3: Density shapes favoring the standard gamma kernel estimator. Schematic densities for which the standard gamma kernel estimator in (2) and (3) should be preferred over the modified version in (2) and (8) according to the shape restriction (12). Left figure: condition (12) is satisfied globally for $x > 2b$ and for $x \leq 2b$ condition (13) holds if f_X can be bounded by cx^{-3} in this area. Right figure: condition (12) can be satisfied locally to the left of the mode.

importance in finite samples, in particular for smaller sample sizes. It can be easily shown, that a pole is a sufficient condition, but the same logic applies to all densities with $f'_X < -c < 0$, c being not too small and $f''_X \geq 0$ close to the boundary.

Apart from these pronounced cases at the boundary, any density whose support is unbounded from the right will be convex and decreasing for large x in order to be integrable. In this situation, the asymptotic variance regimes are identical for both gamma-type estimators. In the asymptotic bias, independent from the rate of decay of f_X , the upper bound of (12) always holds in these regions. For very large x , however, slopes and curvature values are generally small, yielding overall small biases for any kernel-type estimator, such that a measurable advantage of the standard gamma kernel estimator over its modified counterpart might disappear. Besides these convex cases, unimodal densities are concave around the mode and increasing to the left of the mode (see Figure 3). Also in this area, the use of the standard gamma kernel estimator might be recommendable. In finite samples, however, observed differences are rather small even in the extreme case of a strictly concave density between zero and the mode.

Moreover, also in the boundary region for $x \in [0, 2b)$, the standard gamma

kernel estimator can outperform the modified one, if

$$|f'_X(x) + 0.5xf''_X(x)| < |f'_X(x)\xi_b(x)|. \quad (13)$$

As $\xi_b < 1$, this can occur for densities f_X with opposite sign of f'_X and f''_X . Thus, in some pole situations satisfying (12), the standard gamma kernel is superior to the modified one due to $|\xi_b(x)| |1 + 0.5xf''_X(x)/f'_X(x)|^{-1} > 1$ with $\xi_b(x) = (1 - \alpha b) / (1 + b + c_\alpha)$, where $c_\alpha > 0$ for any $x = \alpha b$ in the boundary region. In particular, this is satisfied for densities f_X which can be approximated by cx^{-1} or cx^{-2} for $c > 0$ near the boundary. However, as the boundary region is vanishingly small, its influence on the overall estimation results is negligible (compare the simulation results in Section 3).

In practice, it is therefore important to detect pole situations in advance in order to choose the best performing estimator among standard and modified gamma kernel estimators. We propose a simple but reliable measure to check for poles as opposed to standard cases. If f_X has a pole at zero, it is the relative convergence and consistency of the estimator \hat{f}_X which is of main importance in order to judge if the correct order of decay is detected. See, e.g., Robinson and Henry (2003) for how this is important regarding consistent estimation of the long memory parameter in long range dependent time series. Thus, it must hold that $|\hat{f}_X(x)/f_X(x) - 1| = o_P(1)$. The governing term in the stochastic expansion for the right hand side controlling convergence is $x \frac{f'_X(x)}{f_X(x)}$, which we write as $x D(x)$. See the proof of Theorem 5.3. in Bouezmarni and Scaillet (2005). The practically most important pole situations occur for densities which have or can be bounded by densities with hypergeometric decay from zero, i.e. $f_X(x) = bx^{-\alpha}$ with $b < 0$ and $0 < \alpha < 1$ (the cases with $\alpha > 1$ are excluded by f_X being a density). Here, the quantity $x D(x)$ equals the constant $-\alpha$ irrespective of the scaling b .

For distinguishing a pole situation from a no-pole situation, it is favorable to study $D(x)$ directly to ensure sufficient power of the criterion against alternatives. Therefore, we estimate $D(x)$ by exploiting the simple relation

$$D(x) = \frac{f'_X(x)}{f_X(x)} = \frac{d}{dx} \ln f_X(x). \quad (14)$$

Note that for x approaching 0, in a pole situation $D(x)$ is significantly negative, approaching infinity at rate $\frac{-\alpha}{x}$ in case of densities decreasing with hypergeometric speed and -1 for exponential-type behavior. In all other set-

tings where the modified gamma kernel is the method of choice, $D(x)$ is significantly positive. As a criterion, $D(x)$ combines properties of the density and its slope to distinguish the pole situation from other density shapes. This is more powerful than checking density and slope separately in isolation. In practice, $D(x)$ can be estimated by the difference quotient based on modified gamma kernels

$$\widehat{D}(x) = \frac{\ln \widehat{f}_X^{\gamma m}(x+b) - \ln \widehat{f}_X^{\gamma m}(x)}{b}, \quad (15)$$

where $b > 0$ is the same bandwidth as for the density estimates at x and $x + b$. For the practical scope of this paper, it is sufficient to work with a rough criterion checking if $\widehat{D}(x)$ is significantly negative or not. Developing a novel formal test for the H_0 of a hypergeometric pole situation is beyond the scope of this paper. We conjecture that, using the results in Fernandes and Grammig (2005) for specification testing in the simple density case, the corresponding asymptotic distribution of the centered test statistic $nb^2 \left(\widehat{D}(x) + \frac{\alpha}{x} \right)$ could be derived. However, as calculations are quite involved and should be complemented with a valid bootstrap approximation scheme for finite samples, we leave this for future research and a paper on its own.

2.3. Refined Estimation with Modified Gamma Kernels

In cases where we can exclude a pole at the boundary, the modified gamma kernel generally should be the method of choice in terms of best asymptotic performance. In the literature, its chosen form in particular in the boundary region has mainly been justified by (computational) convenience. However, our simulation results clearly indicate that alternative flexible specifications can significantly improve upon the performance of standard modified gamma kernels.

In particular, we propose simple refined versions of the modified gamma kernel, including an additional specification parameter c that allows for higher accuracy if appropriately chosen in a data-driven way. We study two types of refined modified gamma kernels, i.e.

$$\rho_b^{v_I}(x) = \begin{cases} \left[\frac{1}{4} \left(\frac{x}{bc} \right)^2 + 1 \right] [c + 2b(1 - c)] & \text{if } x \in [0, 2bc), \\ \frac{x}{bc} (c + 2b - x) & \text{if } x \in [2bc, 2b), \\ x/b & \text{if } x \in [2b, \infty), \end{cases} \quad (16)$$

and

$$\rho_b^{v_{II}}(x) = \begin{cases} \frac{1}{4} \left(\frac{x}{bc} \right)^2 + 1 & \text{if } x \in [0, 2bc), \\ x/(bc) & \text{if } x \in [2bc, \infty), \end{cases} \quad (17)$$

where $c \in (0, 1]$ with $c = 1$ yielding the original parameterization in both cases. Specification v_I shifts the boundary regime below one and introduces a flexible quadratic middle part. In the latter regime, for $\rho_b(x) > x/b$ we have that $x/b < \rho_b^{v_I}(x) < \rho_b(x)$ if

$$\frac{x}{b} \frac{2b - x}{\rho_b(x) - x/b} < c < 1, \quad x \in [2bc, 2b), \quad (18)$$

where $\rho_b(x)$ is defined as in (8). Importantly, fulfillment of the condition implies that specification v_I is closer to the theoretically optimal situation with the mean of the kernel being at the observation point as compared to the original modified gamma kernel. The second alternative, v_{II} , keeps two regimes and the general structure of the original specification, but shrinks the boundary region proportionally to the value of the tuning parameter c . This modification also affects asymptotics in the interior of the support, as the mean of the kernel equals x/c and hence, only in the trivial case $c = 1$ coincides with the point of estimation.

Figure 4 shows plots of $\rho_b(x)$ based on the specification proposed by Chen (2000) along with the above refined versions for different values of the constant c and using the bandwidths of two DGPs from the simulation study in Section 3. In addition, we include x/b , which corresponds to the interior component of the original specification and implies a gamma kernel with mean at the point of estimation. In its middle regime, $\rho_b^{v_I}$ is closer to x/b than the original specification for $c = 0.6$ in the right and for both values of c in the left figure, as in these cases condition (18) is satisfied. Close to the boundary, the shape function of specification v_I takes values below

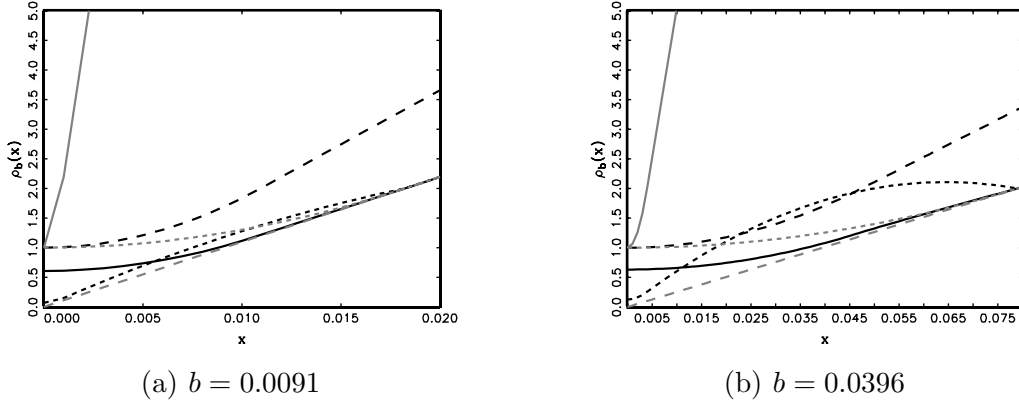


Figure 4: Shape parameter $\rho_b(x)$ of modified gamma kernel. Black solid and short-dashed line: $c = 0.6$ and $c = 0.05$ for refined kernel v_I (see (16)). Grey solid and short-dashed line: $c = 0.6$ and $c = 0.05$ for refined kernel v_{II} (see (17)). Black long-dashed line: original modified kernel (see (8)). Grey long-dashed line: interior regime of original specification and refined version $v_I, x/b$. Bandwidths of the modified gamma kernel estimator for two DGPs from the simulation study in Section 3 are used.

one, implying that the resulting gamma densities and thus, gamma kernels are unbounded at the origin (see Figure 5). However, the finite sample study below clearly reveals that this specification outperforms the original modified and the refined version v_{II} in all settings where a modified gamma kernel should be applied.

For a feasible implementation of these refined estimators, we provide an automatic procedure to select the tuning parameter c : for a fixed bandwidth b , we determine the threshold $x^c = b\kappa$ for which the two MSE expressions of the modified gamma kernel in (10) coincide. Then, the optimal value of c can then be obtained as $c^* = \kappa/2 = x^c/(2b)$. In practice, this approach requires minimizing the following objective function in $0 \leq x \leq 2b$:

$$\mathcal{M}(x) = \left\{ \left[\xi_b(x) b f'_X(x) \right]^2 + \frac{f_X(x)}{nb} \mathcal{C}_b(x) - \left[\frac{1}{2} x f''_X(x) b \right]^2 - \frac{f_X(x)}{2\sqrt{\pi}} (xb)^{-1/2} n^{-1} \right\}^2. \quad (19)$$

Evaluation of the objective function requires estimates of the unknown density and its first two derivatives. $f_X(x)$ and $f'_X(x) = D(x) f_X(x)$ can

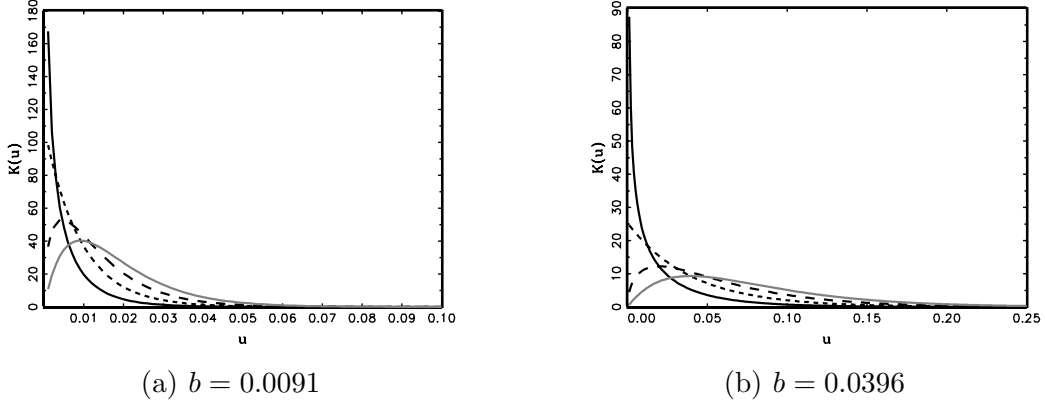


Figure 5: Gamma kernel depending on shape parameter. Gamma kernel $K_{\rho_b(x),b}^\gamma(u)$ for different values of shape parameter ρ_b . Black solid line: $\rho_b = 0.5$. Black short-dashed line: $\rho_b = 1$. Black long-dashed line: $\rho_b = 1.5$. Grey solid line: $\rho_b = 2$. Bandwidths of the modified gamma kernel estimator for two DGPs from the simulation study in Section 3 are used.

be estimated using the original modified gamma kernel. An estimate of $f_X''(x)$ can be obtained by differentiating, e.g., the standard gamma kernel estimator:

$$\begin{aligned} \hat{f}_X''^\gamma(x) &= \frac{1}{nb^2} \sum_{i=1}^n \frac{\partial^2}{\partial x^2} K_{x/b+1,b}^\gamma(X_i), \\ &= \frac{1}{nb^2} \sum_{i=1}^n K_{x/b+1,b}^\gamma(X_i) \left\{ \left[\ln(X_i/b) - \psi(x/b+1) \right]^2 - \psi_1(x/b+1) \right\}, \end{aligned} \quad (20)$$

where $\psi(u) = (d/du) \ln \Gamma(u)$ and $\psi_1(u) = (d^2/du^2) \ln \Gamma(u)$ denote the digamma and trigamma function, respectively.

3. Simulation Study

For a complete picture, we compare standard, modified and refined gamma kernel estimators to standard boundary corrected versions of the symmetric fixed kernel density estimator (1) for a wide range of test densities representing all potential types of shapes near the boundary. This also complements simulation studies in the literature for the two original gamma kernels, such as Chen (2000) which only focuses on very specific density settings and Hag-

mann and Scaillet (2007) which is restrictive in the range of fixed boundary kernel competitors.

All fixed kernels are based on the Epanechnikov kernel $K(u) = 3/4(1 - u^2)\mathbb{I}(-1 \leq u \leq 1)$, where $\mathbb{I}(\cdot)$ denotes an indicator function limiting the support of K to $[-1, 1]$. In particular, we report results for the following five competing fixed kernel adjustments.

The reflection estimator proposed by Schuster (1958) has the form

$$\hat{f}_X^{\text{Refl}}(x) = \frac{1}{nb} \sum_{i=1} \left[K\left(\frac{x - X_i}{b}\right) + K\left(\frac{x + X_i}{b}\right) \right]. \quad (21)$$

In the inside of the support for $x \geq 2h$, it coincides with the standard kernel density estimator \hat{f}_X^{Fixed} in (1).

Karunamuni and Alberts (2005) generalize the reflection estimator (21) to

$$\hat{f}_X^{\text{GRefl}}(x) = \frac{1}{nb} \sum_{i=1} \left[K\left(\frac{x - \hat{g}_\nu(X_i)}{b}\right) + K\left(\frac{x + \hat{g}_\nu(X_i)}{b}\right) \right], \quad (22)$$

where $\hat{g}_\nu(y) = y + (1/2) \hat{d}_0 k'_\nu y^2 + \lambda_0 (\hat{d}_0 k'_\nu)^2 y^3$, with \hat{d}_0 being an estimate of $d_0 := f'_X(0) / f_X(0)$ and

$$k'_\nu = 2 \int_\nu^1 (u - \nu) K(u) du \Big/ \left(\nu + 2 \int_\nu^1 (u - \nu) K(u) du \right), \quad \nu := x/b, \quad (23)$$

while λ_0 is a constant such that $12 \lambda_0 > 1$. We estimate d_0 as outlined in Section 2.2 and 3 of Karunamuni and Alberts (2005).

In the cut-and-normalized estimator \hat{f}_X^{CaN} introduced by Gasser and Müller (1979), the kernel function K for the boundary region is truncated at ν and normalized, ensuring integration to unity. For the Epanechnikov kernel, it has the form

$$K^{\text{CaN}}(u) = \frac{(1 - u^2)}{\int_{-1}^\nu (1 - u^2) du} \mathbb{I}_{\{-1 \leq u \leq \nu\}}. \quad (24)$$

General boundary corrected estimators \hat{f}_X^{Bound} (see, e.g., Jones, 1993) replace the standard kernel function in the boundary region by a modified

version K^{Bound} , which is chosen to meet the following conditions:

$$\int_{\nu}^1 K^{\text{Bound}}(u) du = 0, \quad \int_{-1}^{\nu} K^{\text{Bound}}(u) du < \infty, \quad \int_{-1}^{\nu} K^{\text{Bound}}(u) u du = 0. \quad (25)$$

We use the boundary kernel based on the Epanechnikov kernel, which has the following form:

$$K^{\text{Bound}}(u) = 12 \frac{(1+u)}{(1+\nu)^4} \left[\frac{3\nu^2 - 2\nu + 1}{2} + u(1-2u) \right] \mathbb{I}_{\{-1 \leq u \leq \nu\}}. \quad (26)$$

A method that corrects for the possible negativity of the boundary kernel estimates was proposed, e.g., by Jones and Foster (1996). The estimator has the following form:

$$\hat{f}_X^{\text{JF}}(x) = \hat{f}_X^{\text{CaN}}(x) \exp \left\{ \frac{\hat{f}_X^{\text{Bound}}(x)}{\hat{f}_X^{\text{CaN}}(x)} - 1 \right\}. \quad (27)$$

We compare the performance of the estimators for seven different density functions with nonnegative support, which reflect the variety of practically relevant types of shapes on left-bounded support. The densities of DGP 1 and DGP 2 are entirely decreasing and convex with DGP 2 exhibiting pole behavior at zero. The remaining densities are increasing near the boundary. For DGP 3 and 4, the density is locally convex in the boundary region, while for 5,6 and 7 it is concave with varying degree of steepness. The corresponding density shapes are depicted in Figure 6. All DGPs are generated from different specifications of the flexible generalized F distribution, which is based on a gamma mixture of the generalized gamma distribution (see, e.g., Lancaster, 1997). Its marginal density function is given by

$$f_x(x) = \frac{a x^{a m - 1} [\eta + (x/\lambda)^a]^{(-\eta - m)} \eta^\eta}{\lambda^{a m} \mathcal{B}(m, \eta)}, \quad (28)$$

where $a > 0, m > 0, \eta > 0$ and $\lambda > 0$. $\mathcal{B}(\cdot)$ describes the full Beta function with $\mathcal{B}(m, \eta) := \frac{\Gamma(m)\Gamma(\eta)}{\Gamma(m+\eta)}$. Table 1 shows the values of the shape parameters a, m and η for the seven DGPs considered. To ensure comparability across the different DGPs, the expectation is restricted to one by setting the scale

Table 1: Data generating processes for simulation study. DGPs are generated from i.i.d. samples of different specifications of the generalized F distribution (28). We use the following tuples of shape parameters a , m and η . The scale parameter λ is chosen such that the expectation of each DGP is normalized to one. Corresponding shapes of the densities are depicted in Figure 6.

DGP	a	m	η
1	1	1	∞
2	0.9	0.7	1.2
3	14	0.2	0.5
4	35	0.08	0.1
5	0.8	2	∞
6	0.55	3	5
7	5	0.3	∞

parameter λ equal to

$$\lambda = \eta^{-1/a} \frac{\Gamma(m) \Gamma(\eta)}{\Gamma(m + 1/a) \Gamma(\eta - 1/a)}. \quad (29)$$

From each DGP, we draw 1000 random samples $\{X_i\}_{i=1}^n$ of size $n = 400$ and $n = 4000$. To minimize the effects of sampling variation, we follow Zhang (2010) and select the optimal bandwidth for each estimator and DGP by minimizing the integrated mean squared error (IMSE)

$$\text{IMSE}\{\hat{f}_X(x)\} = \frac{1}{1000} \sum_{r=1}^{1000} \int_{\tau}^{\infty} \{f_X(x) - \hat{f}_X^r(x)\}^2 dx, \quad (30)$$

where τ is a small number and $\hat{f}_X^r(x)$ denotes the density estimate for the r th simulated sample. Bandwidth selection is conducted using the sample size $n_b = 200$, which requires multiplying the resulting bandwidths by the factor $(n/n_b)^{-1/5}$ for the subsequent analysis. The rescaled bandwidths for $n = 400$ and $n = 4000$ are reported in Table 2. The two gamma kernel estimators exhibit noticeably smaller bandwidths in comparison to the other estimators, which can be explained by the reduced variance of the former in the interior part of the support.

Table 3 and 4 report the IMSEs of the different estimators for the seven DGPs and two samples sizes. IMSEs are computed over the interval $[0, 2]$. For DGPs 3 to 7, we additionally consider shorter intervals that encompass

Table 2: Bandwidths. Bandwidths chosen by minimizing the mean integrated squared error (30) using simulated samples with $n = 200$. The following estimators are used. Gam and Gam_m: basic and modified gamma kernel estimator. Fixed: fixed kernel estimator based on the epanechnikov kernel. Refl: reflection estimator. GRefl: generalized reflection estimator. CaN: cut-and-normalized estimator. Bound: boundary kernel estimator. JF: Jones-Foster estimator.

Est.	DGP 1	DGP 2	DGP 3	DGP 4	DGP 5	DGP 6	DGP 7
$n = 400$							
Gam	0.0768	0.0042	0.0096	0.0088	0.0571	0.0319	0.0308
Gam _m	0.1163	0.0166	0.0099	0.0091	0.0634	0.0396	0.0336
Fixed	0.1821	0.0176	0.2058	0.1820	0.2678	0.0888	0.4015
Refl	0.4643	0.0391	0.2054	0.1818	0.3569	0.2144	0.3609
GRefl	0.7497	0.0499	0.2066	0.1829	0.3210	0.2875	0.3953
CaN	0.4223	0.0307	0.2044	0.1808	0.4308	0.1868	0.3494
Bound	0.7471	0.0086	0.2064	0.1825	0.3824	0.3141	0.4024
JF	0.4223	0.0307	0.2044	0.1808	0.4308	0.1868	0.3494
$n = 4000$							
Gam	0.0485	0.0027	0.0061	0.0055	0.0360	0.0201	0.0195
Gam _m	0.0734	0.0104	0.0062	0.0058	0.0400	0.0250	0.0212
Fixed	0.1149	0.0111	0.1299	0.1148	0.1689	0.0561	0.2533
Refl	0.2930	0.0247	0.1296	0.1147	0.2252	0.1353	0.2277
GRefl	0.4730	0.0315	0.1304	0.1154	0.2025	0.1814	0.2494
CaN	0.2664	0.0194	0.1290	0.1141	0.2718	0.1179	0.2204
Bound	0.4714	0.0054	0.1302	0.1152	0.2413	0.1982	0.2539
JF	0.2664	0.0194	0.1290	0.1141	0.2718	0.1179	0.2204

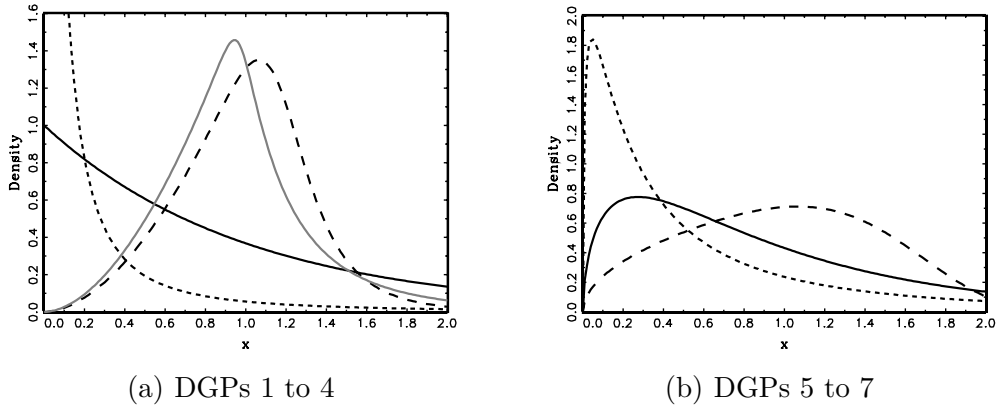


Figure 6: Densities corresponding to different DGPs. Densities corresponding to tuples of shape parameters in Table 1. Left: DGP 1 (black solid), DGP 2 (black short-dashed), DGP 3 (black long-dashed) and DGP 4 (grey solid). Right: DGP 5 (black solid), DGP 6 (black short-dashed) and DGP 7 (black long-dashed).

and exclude the mode of the distribution, respectively. Three major results are apparent. First, in a general comparison with the standard fixed kernel adjustments, gamma kernel estimators appear to offer a satisfactory performance. They are clearly more precise for DGPs 2, 5 and 6, while yielding similar (or only slightly higher) IMSEs in the remaining cases. In particular, the single largest improvement in favor of the (standard) gamma kernel is achieved in the pole scenario of DGP 2. Note that when the applied polynomial transformation for the method of Marron and Ruppert (1994) was close to the true pole behavior, we could also construct a fixed kernel estimator with a similar or even better precision for DGP 2. Corresponding results, however, were not robust to deviations of the transformation from the true density shape near zero implying a high risk of extremely large IMSEs in practice. Due to the tailored construction of the above method for pole situations only, also the IMSE records for any other form of the density were largely inferior to the rest. Therefore, we do not report results for this estimator.

Second, the simulation evidence confirms the relationship between the performance of the standard and modified gamma kernel estimator and the shape of the underlying density. If the latter has first and second derivatives of opposing sign in the interior of the support, as is the case for DGPs 3, 4, 6 and 7 in the subinterval to the right of the mode, the standard gamma

kernel yields noticeably lower IMSEs (see bottom panel). When considering the entire interval $[0, 2]$, the standard gamma kernel is more precise for DGPs 2 and 6 with the most striking gains occurring in the former scenario, as it corresponds to a globally convex density with pole at zero. Finally, the above relation breaks down within the boundary region due to the involvement of the factor $\xi_b(x)$ in the asymptotic bias (see (9)). For DGPs 5 and 6, the modified gamma kernel implies lower IMSEs over the leftmost subinterval in which the corresponding densities are increasing and concave (see lower top panel).

The simulation results stress the importance of determining pole situations in advance, which can be achieved by examining the normalized density derivative $D(x)$ in the boundary region. We estimate the latter as in (15) using the modified gamma kernel for the points $x \in \{0, b, 2b\}$, where b is the bandwidth of the corresponding estimator. Table 5 reports descriptive statistics of the estimates for $n = 400$. In case of DGP 2, these estimates are highly negative at all three points, demonstrating that our simple method is able to detect a pole at zero. We obtain negative estimates at all or at distinct points also for DGPs 1 and 6, but their magnitude is considerably lower than in the above true pole scenario.

As was argued in Section 2.2, whenever no pole situation has been detected, the modified gamma kernel in its original or refined form should be used. The IMSEs of the three corresponding estimators are displayed in Table 6. For the refined kernels v_I and v_{II} , a set of values for the threshold c is considered. To ensure comparability, we apply the bandwidths b of the original modified gamma kernel to all estimators and also use $2b$ as the upper integration limit in the IMSE calculations. The main finding is that the refined kernel v_I exhibits a high precision in all situations for which the modified kernel should be considered, i.e. all DGPs except the second one. The improvement with respect to the original specification is particularly pronounced, accompanied by low optimal values of the constant c , in case of densities with concave shape near the boundary, as in DGPs 5,6 and 7. Further, the refined kernel v_{II} is at roughly the same level as the traditional parameterization and even yields the lowest IMSE for DGP 1 when $n = 400$. However, recall that this specification makes the boundary region smaller and has neither its mean nor mode at the point of estimation for $x > 2bc$ (see Section 2.3). These properties cause a vastly lower precision compared to the other specifications in the interior part of the support. Corresponding simulation results are available upon request.

Table 3: Integrated mean-squared errors (n=400). For DGP 3, 4 and 7, limits x_1 and x_2 are chosen such that $[x_1, x_2]$ encompasses the mode. $x_1 \in \{0.888, 0.600, 0.500\}$ and $x_2 \in \{1.292, 1.090, 1.700\}$. For DGP 5 and 6, $x_1 = x_2$ is chosen such that $[0, x_1]$ includes the mode, where $x_1 = x_2 \in \{0.600, 0.200\}$. For estimators, see Table 2. Results are re-scaled by the factor 10^3 .

Est.	DGP 1	DGP 2	DGP 3	DGP 4	DGP 5	DGP 6	DGP 7
$0 \leq x \leq 2$							
Gam	4.185	75.151	8.857	9.759	5.828	14.572	5.286
Gam _m	3.575	279.733	8.720	9.623	5.422	14.879	4.575
Fixed	17.659	287.118	7.293	8.63	7.182	26.125	3.462
Refl	3.854	320.621	7.309	8.645	9.815	16.738	4.943
GRefl	2.418	302.933	7.267	8.612	8.093	19.334	4.065
CaN	4.171	177.666	7.340	8.67	10.16	17.46	5.308
Bound	3.039	356.335	7.279	8.621	6.651	18.096	3.594
JF	4.259	923.101	7.274	8.612	7.235	17.629	3.792
$0 \leq x \leq x_1$							
Gam			2.880	1.729	4.691	11.902	1.804
Gam _m			2.553	1.502	4.330	11.59	1.501
Fixed			2.015	1.125	4.991	17.248	0.934
Refl			2.037	1.143	8.285	13.032	2.309
GRefl			1.977	1.095	6.342	16.019	1.529
CaN			2.083	1.178	8.956	13.339	2.619
Bound			1.993	1.109	5.25	14.616	1.066
JF			2.017	1.120	6.030	13.508	1.104
$x_1 \leq x \leq x_2$							
Gam			4.702	6.416			3.224
Gam _m			4.304	6.038			2.549
Fixed			3.788	5.316			2.190
Refl			3.783	5.312			2.303
GRefl			3.799	5.333			2.200
CaN			3.770	5.295			2.358
Bound			3.796	5.326			2.189
JF			3.770	5.295			2.358
$x_2 \leq x \leq 2$							
Gam			1.220	1.573	1.136	2.670	0.258
Gam _m			1.806	2.039	1.092	3.289	0.525
Fixed			1.433	2.134	2.190	8.877	0.339
Refl			1.432	2.136	1.530	3.706	0.330
GRefl			1.435	2.129	1.751	3.315	0.336
CaN			1.431	2.141	1.204	4.122	0.331
Bound			1.434	2.131	1.401	3.479	0.339
JF			1.431	2.141	1.204	4.122	0.331

Table 4: Integrated mean-squared errors (n=4000). For DGP 3, 4 and 7, limits x_1 and x_2 are chosen such that $[x_1, x_2]$ encompasses the mode. $x_1 \in \{0.888, 0.600, 0.500\}$ and $x_2 \in \{1.292, 1.090, 1.700\}$. For DGP 5 and 6, $x_1 = x_2$ is chosen such that $[0, x_1]$ includes the mode, where $x_1 = x_2 \in \{0.600, 0.200\}$. For estimators, see Table 2. Results are re-scaled by the factor 10^3 .

Est.	DGP 1	DGP 2	DGP 3	DGP 4	DGP 5	DGP 6	DGP 7
$0 \leq x \leq 2$							
Gam	1.011	21.601	2.246	2.758	2.069	6.924	1.218
Gam _m	0.679	161.086	2.237	2.76	1.734	7.307	0.986
Fixed	8.122	46.145	1.331	1.683	1.960	8.504	0.734
Refl	0.803	154.026	1.332	1.684	4.415	10.797	1.203
GRefl	0.407	234.486	1.329	1.685	2.548	12.980	0.822
CaN	0.890	56.600	1.334	1.682	5.443	10.075	1.318
Bound	0.471	62.457	1.329	1.684	2.106	10.593	0.684
JF	0.585	616.087	1.327	1.676	2.663	8.142	0.721
$0 \leq x \leq x_1$							
Gam			0.450	0.271	1.831	6.484	0.322
Gam _m			0.349	0.207	1.532	6.567	0.216
Fixed			0.360	0.193	1.592	7.029	0.267
Refl			0.362	0.194	4.149	10.148	0.723
GRefl			0.355	0.190	2.248	12.327	0.354
CaN			0.367	0.198	5.227	9.364	0.830
Bound			0.357	0.191	1.859	9.886	0.216
JF			0.360	0.192	2.447	7.431	0.234
$x_1 \leq x \leq x_2$							
Gam			1.495	2.200			0.826
Gam _m			1.337	2.055			0.567
Fixed			0.721	1.118			0.405
Refl			0.720	1.116			0.421
GRefl			0.723	1.124			0.407
CaN			0.717	1.11			0.430
Bound			0.722	1.121			0.405
JF			0.717	1.110			0.430
$x_2 \leq x \leq 2$							
Gam			0.293	0.281	0.238	0.440	0.071
Gam _m			0.542	0.488	0.202	0.741	0.202
Fixed			0.239	0.361	0.369	1.475	0.062
Refl			0.239	0.361	0.266	0.650	0.058
GRefl			0.240	0.360	0.301	0.653	0.061
CaN			0.239	0.362	0.216	0.711	0.058
Bound			0.239	0.361	0.247	0.706	0.062
JF			0.239	0.362	0.216	0.711	0.058

Table 5: Summary statistics of normalized density derivative. Descriptives for estimate of the ratio $D(x) := f'(x)/f(x)$ based on the modified gamma kernel. The estimator from equation (15) is used. $n = 400$.

x	DGP 1	DGP 2	DGP 3	DGP 4	DGP 5	DGP 6	DGP 7
<i>Mean</i>							
0	-0.226	-13.982	73.923	80.433	1.899	1.265	4.71
b	-0.711	-27.341	182.844	205.189	3.26	0.756	8.741
$2b$	-0.941	-23.57	185.301	198.408	1.892	-1.558	6.763
<i>1st Quartile</i>							
0	-0.399	-15.110	67.995	73.900	1.473	0.737	2.707
b	-1.017	-29.185	165.094	184.470	2.467	-0.257	4.562
$2b$	-1.180	-25.188	161.913	172.373	1.247	-2.386	3.800
<i>Median</i>							
0	-0.220	-13.928	75.557	82.861	1.922	1.284	4.89
b	-0.727	-27.382	187.737	212.998	3.209	0.710	8.395
$2b$	-0.939	-23.557	191.768	208.193	1.865	-1.568	6.629
<i>3rd Quartile</i>							
0	-0.059	-12.794	81.790	89.863	2.350	1.798	7.020
b	-0.421	-25.602	206.611	235.238	4.025	1.764	12.854
$2b$	-0.703	-21.906	216.830	236.042	2.493	-0.786	9.496

Table 6: Integrated MSE for refined modified gamma KDE v_I & v_{II} . Refined modified gamma kernel estimators as defined in (7) and (16) or (17). $c = 1^*$ denotes original modified gamma kernel from (7) and (8). IMSEs are computed from 0 to $2b$. Bandwidths of the original modified gamma kernel are used.

	c	DGP 1	DGP 2	DGP 3	DGP 4	DGP 5	DGP 6	DGP 7
$n = 400$ (IMSE $\times 10^4$)								
v_I	1*	18.230	1971.5	0.005	0.009	24.452	99.402	2.713
	0.9	18.389	2238.2	0.005	0.008	22.112	98.176	2.555
	0.8	18.927	3280.7	0.005	0.008	19.936	97.139	2.416
	0.7	19.976	6045.5	0.004	0.007	17.94	96.462	2.299
	0.6	21.776	13836.5	0.004	0.007	16.123	96.310	2.201
	0.3	39.301	16309119	0.004	0.007	11.443	96.476	1.991
	0.1	74.542	3193545	0.004	0.007	9.150	69.093	1.872
	0.05	99.107	29681669	0.004	0.007	18.179	45.087	2.162
0.01	623.499	3640.6	0.008	0.012	72.511	144.333	10.431	
v_{II}	0.9	17.878	1453.3	0.006	0.01	23.301	97.185	2.722
	0.8	18.157	1040.2	0.007	0.011	22.507	95.373	2.78
	0.7	19.768	837.2	0.008	0.013	22.47	94.715	2.937
	0.6	24.05	996.3	0.009	0.015	23.755	96.878	3.285
	0.3	104.500	6653.9	0.027	0.042	43.068	195.018	8.734
	0.1	629.167	24190.1	0.364	0.530	81.172	874.974	48.989
	0.05	1115.94	32319.5	3.483	5.224	170.476	1460.69	105.8
	0.01	1688.05	38771.3	69.245	70.217	321.568	2185.42	48.598
$n = 4000$ (IMSE $\times 10^5$)								
v_I	1*	25.397	10185.6	0.002	0.002	94.207	594.231	5.050
	0.9	23.982	16235.4	0.002	0.002	80.85	562.997	4.439
	0.8	23.446	29262.9	0.002	0.001	68.844	533.361	3.912
	0.7	24.057	55516.9	0.001	0.001	58.242	506.235	3.472
	0.6	26.498	110274.9	0.001	0.001	49.013	483.124	3.115
	0.3	109.444	16058082	0.001	0.001	27.206	431.343	2.493
	0.1	721.532	561573	0.001	0.001	11.743	283.302	2.029
	0.05	740.051	57227048	0.001	0.001	31.993	131.333	2.011
0.01	1716.07	6091.9	0.002	0.002	523.996	244.364	16.592	
v_{II}	0.9	25.709	5653.4	0.002	0.002	88.817	571.585	5.026
	0.8	27.903	2185.2	0.002	0.002	86.931	550.769	5.212
	0.7	33.997	682.4	0.003	0.003	91.895	534.382	5.827
	0.6	47.993	2474.8	0.003	0.003	108.945	526.934	7.271
	0.3	306.934	53804.8	0.009	0.011	334.800	750.698	31.256
	0.1	2502.0	207647.9	0.145	0.209	634.147	3412.3	212.589
	0.05	5517.4	277217.4	1.424	2.168	757.340	6670.1	540.434
	0.01	10682.7	335603.3	373.201	424.930	1566.361	12161.6	433.552

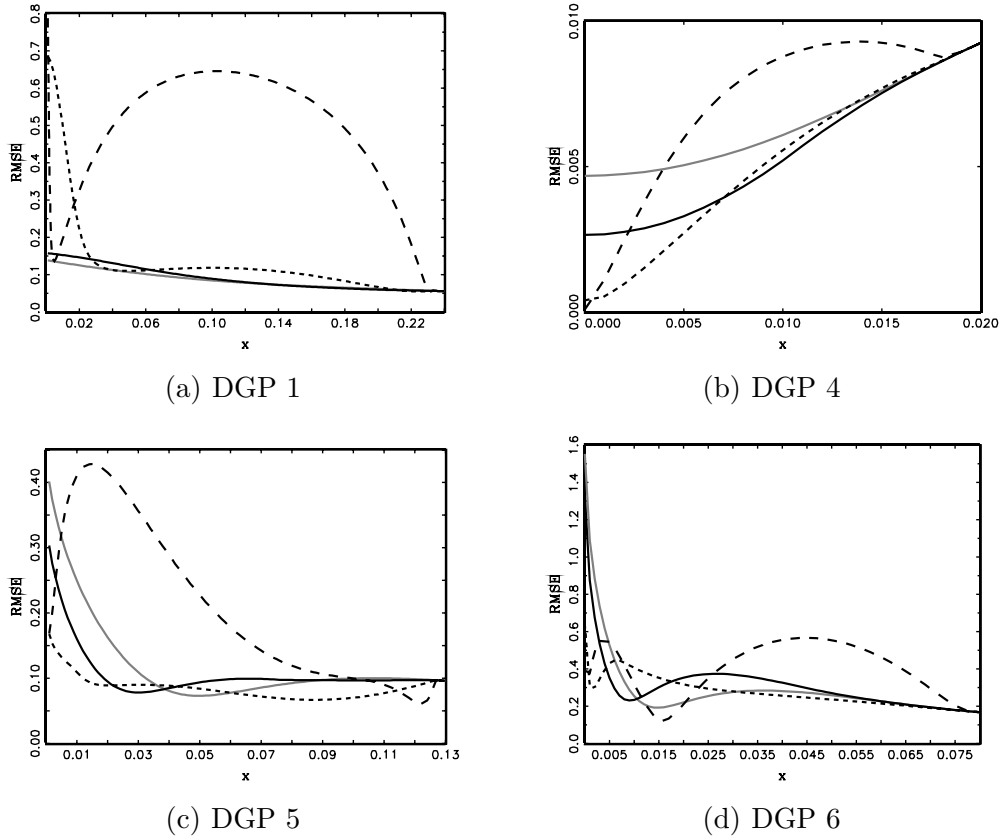


Figure 7: RMSE of refined modified gamma KDE v_l . Refined modified gamma kernel v_l as defined in (7) and (16). Black solid line: $c = 0.6$. Black short-dashed line: $c = 0.1$. Black long-dashed line: $c = 0.01$. Grey solid line: $c = 1^*$ (original modified gamma kernel). $n = 400$. Bandwidths of the original modified gamma kernel are used.

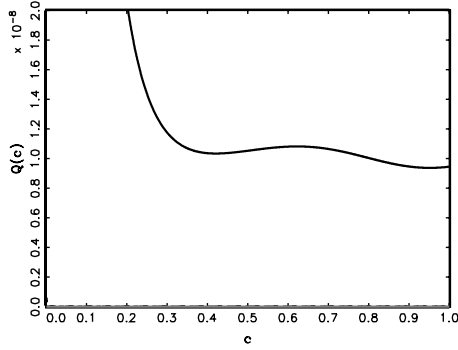
Finally, Table 6 shows that the performance of the refined modified gamma kernel estimators is highly dependent on the value of the threshold c . This is underlined by Figure 7, which depicts plots of the root mean squared errors (RMSEs) of the estimators based on the original modified gamma kernel and the refined version v_l for several values of c . The plots also illustrate that the choice of c determines for which part of the support the original estimator can or cannot be outperformed. E.g., in case of DGP 4, specification v_l almost consistently exhibits lower RMSEs for $c = 0.6$ or $c = 0.1$, while providing precise estimates only in a small neighborhood of $x = 0$ if $c = 0.01$.

Since, in practice, the constant c has to be chosen ex-ante, we exam-

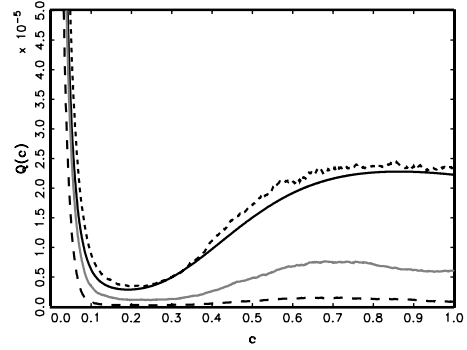
ine how well the data-driven method introduced in Section 2.3 can “track” the optimal values according to Table 6. We estimate the unknown quantities entering the objective function (19) as was outlined above. Figure 8 displays averages, medians and quartiles of the resulting estimates of the (transformed) objective function $\mathcal{Q}(c) := \mathcal{M}(2bc)$, where b is the bandwidth of the modified gamma kernel. A comparison with the IMSEs from Table 6 shows that for DGPs 5, 6 and 7 the means, in particular, have local minima close to the values of c yielding the lowest IMSEs of the estimator based on the refined modified kernel v_1 . For DGP 4, finding a unique minimum is more difficult, which corresponds to the fact that several values of c imply equal IMSEs. These results suggest that, if suitable starting values are chosen, the above approach can determine the optimal value of c with reasonable precision.

To highlight the increased gains from employing the refined modified gamma kernel v_1 in a multivariate context, we compare the finite sample performance of the product kernel version of the respective estimator in (7) based on the modified kernel (8) and the refined modified kernel (16). We illustrate the effect in a simulation of random samples of size $n = 400$ from two types of bivariate DGPs with different dimensionality of boundary problems. The first one is based on DGPs 3-7 from the univariate study, each combined with a truncated normal distribution with $\mu = 6$ and $\sigma = 1$ under an independence assumption. This setting reflects a situation in which only one boundary problem is present and is motivated by the finite sample study in Bouezmarni and Rombouts (2010a). The second setting introduces two boundary problems with both marginals corresponding to one of the DGPs 3-7. We choose the optimal bandwidths for the original modified kernel based on a procedure analogue to the univariate case, while employing the same bandwidths also for the refined version of the kernel.

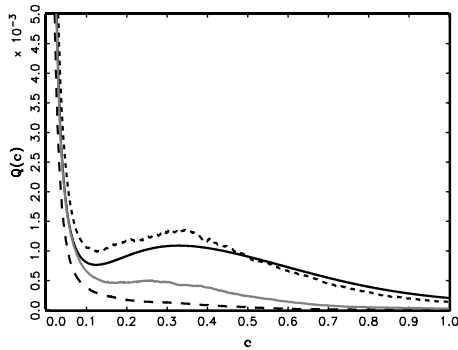
Table 7 exemplarily reports the difference of the IMSEs implied by the original and refined version of the modified kernel for DGP 5. Note that similar results can be observed for every density shape (DGP 3-7) favoring the modified kernel in the univariate setting (see Table 6). The corresponding results are omitted here for the sake of brevity, but are available upon request. In the case of the refined modified kernel, different values of the specification parameters c_1 and c_2 are considered. If these parameters are chosen in an optimal way (see also Figure 8), the refined modified kernel implies a lower IMSE already in the setting with only one boundary problem. These precision gains, however, increase substantially in the scenario with two boundary



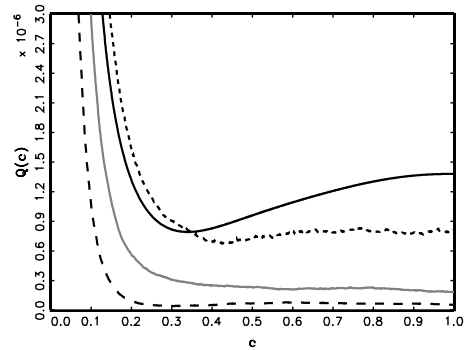
(a) DGP 4



(b) DGP 5



(c) DGP 6



(d) DGP 7

Figure 8: Objective function for choice of c . Mean (black solid), median (grey solid), first (black long-dashed) and third (black short-dashed) quartile of (transformed) objective function for choice of the constant c in the refined modified gamma kernel v_I as defined in (7) and (16). The transformed objective function is $Q(c) := \mathcal{M}(2bc)$, where $\mathcal{M}(x)$ is given in (19) and b denotes the bandwidth of the original modified gamma kernel. $n = 400$.

Table 7: Gains of refined vs. original modified gamma KDE in bivariate case. Difference of IMSEs implied by product kernel estimator based on original modified gamma kernel (8) and its counterpart employing the refined version v_1 in (16). One boundary problem: marginals based on DGP 5 and truncated normal distribution with $\mu = 6$ and $\sigma = 1$. Two boundary problems: both marginals based on DGP 5. In both cases, cross-sectional independence is assumed. Sample size $n = 400$. Bandwidths of the original modified gamma kernel are used.

One boundary problem ($\Delta\text{IMSE} \times 10^{30}$)						
$c_2 \setminus c_1$	1*	0.9	0.7	0.5	0.3	0.1
1*		-0.162	-0.282	-0.259	-0.094	1.095
0.9	-0.053	-0.212	-0.330	-0.307	-0.145	1.021
0.7	-0.143	-0.296	-0.411	-0.389	0.000	0.894
0.5	-0.191	-0.341	-0.453	-0.432	-0.278	0.827
0.3	-0.156	-0.308	-0.422	-0.400	-0.245	0.876
0.1	-0.043	-0.202	-0.321	-0.298	-0.136	1.035
Two boundary problems ($\Delta\text{IMSE} \times 10^7$)						
$c_2 \setminus c_1$	1*	0.9	0.7	0.5	0.3	0.1
1*		0.245	0.770	1.382	2.200	2.876
0.9	0.238	0.455	0.932	1.515	2.345	3.217
0.7	0.758	0.925	1.318	1.849	2.700	3.913
0.5	1.345	1.479	1.815	2.313	3.181	4.624
0.3	2.055	2.193	2.538	3.047	3.927	5.351
0.1	2.708	3.034	3.702	4.411	5.187	5.277

problems. They are particularly pronounced for optimal choices of c_1 and c_2 , while already yielding results superior to those for the original modified kernel given any reported combination of parameters. These findings demonstrate the benefits from using the refined version of the modified gamma kernel when raising the dimension of the boundary problem only from one to two. We expect these gains to grow even further for a multivariate setting with an increasing number of included boundary problems.

4. Application: Intraday Trading Volumes and Return Volatility

To demonstrate the practical relevance of the above methodology, we employ the latter to compute semiparametric estimates of the conditional distributions of high-frequency trading volumes and return volatilities of stocks traded at the New York Stock Exchange (NYSE). Modeling high-frequency

trading volumes is, for instance, relevant for trading strategies replicating the (daily) volume weighted average price (VWAP). Estimates of conditional volatility distributions are crucial for the pricing of volatility derivatives. Examples include options and futures on the CBOE Volatility Index (VIX) trading at the Chicago Board Options Exchange (CBOE).

4.1. Modeling Intraday Trading Volumes

We consider transaction data for Citigroup from the last trading week of February 2009. The raw sample is filtered by deleting transactions that occurred outside regular trading hours from 9:30 am to 4:00 pm, computing cumulated trading volumes over 15 second intervals and removing zero observations, which yields a sample size of 7452. For a detailed discussion of the treatment of zero observations in the context of financial high-frequency data, see Hautsch et al. (2013). To capture the well-known intraday seasonalities of high-frequency trading variables (see, e.g., Hautsch (2004) for an overview), we divide the cumulated volumes by a seasonality component which is pre-estimated employing a cubic spline function.

An important property of the resulting (deseasonalized) trading volumes is the strong persistence, as evidenced by the highly significant Ljung-Box statistics in Table 8. The most widely-used parametric framework for this type of data, see, e.g., Brownlees et al. (2010), is the multiplicative error model (MEM) originally proposed by Engle (2002). Accordingly, we decompose the t -th trading volume, $x_t^{(v)}$, as

$$x_t^{(v)} = \mu_t^{(v)} \varepsilon_t^{(v)}, \quad \varepsilon_t^{(v)} \sim \text{i.i.d. } \mathcal{D}(1), \quad (31)$$

where $\mu_t^{(v)}$ denotes the conditional mean given the past information set $\mathcal{F}_{t-1}^{(v)}$ and is assumed to evolve according to the dynamics described in Appendix A. $\varepsilon_t^{(v)}$ is a disturbance following an unspecified distribution $\mathcal{D}(1)$ with positive support and $E[\varepsilon_t^{(v)}] = 1$. Assuming MEM-type dynamics would allow to apply gamma kernel estimators to trading volumes directly and estimate their unconditional density $f_X(x_t^{(v)})$ consistently (see Bouezmarni and Rombouts, 2010b). Our object of interest, the conditional density given the past information set $\mathcal{F}_{t-1}^{(v)}$, can be estimated semiparametrically in a straightforward way, as the MEM structure implies the basic relationship

$$f_X(x_t^{(v)} | \mathcal{F}_{t-1}^{(v)}) = f_\varepsilon(x_t^{(v)} / \mu_t^{(v)}) / \mu_t^{(v)}. \quad (32)$$

Table 8: Ljung-Box statistics for intraday trading volumes and realized kernel estimates. $Q(l)$: Ljung-Box statistic associated with l lags. The 5% (1%) critical values associated with lag lengths 20, 50 and 100 are 31.41 (37.57), 67.51 (76.15) and 124.34 (135.81). We consider deseasonalized nonzero 15-second trading volumes of Citigroup and realized kernel (RK) estimates for JP Morgan.

	Volume	RK
$Q(20)$	10349.281	5045.309
$Q(50)$	19447.096	9834.944
$Q(100)$	31353.699	14012.591

We consider a two-step approach. First, we estimate $\mu_t^{(v)}$ by exponential QML and generate residuals $\hat{\varepsilon}_t^{(v)} := x_t^{(v)} / \hat{\mu}_t^{(v)}$, which are consistent estimates of the i.i.d errors $\varepsilon_t^{(v)}$ (see, e.g., Drost and Werker, 2004). Second, we estimate $f_\varepsilon(x_t^{(v)} / \mu_t^{(v)})$ nonparametrically employing gamma kernels. The consistency and parametric rate of convergence of the conditional mean estimates enable us to use the MEM residuals as inputs without affecting the asymptotics of the kernel density estimators.

Nonparametric estimation of the error density requires the choice of the appropriate type of gamma kernel, i.e. standard or modified in the original and refined version (specification v_1). To ensure comparability and boundary regions of equal size, we consider the least-squares cross-validation (LSCV) bandwidth of the standard gamma kernel estimator in all cases. In particular, we use the bandwidth b^* that minimizes a nearly unbiased estimate of the integrated mean-squared error, i.e.

$$CV(b) = \frac{1}{n^2} \sum_i \sum_j \int_{\tau}^{\infty} K_{x/b+1,b}^{\gamma}(\hat{\varepsilon}_i^{(v)}) K_{x/b+1,b}^{\gamma}(\hat{\varepsilon}_j^{(v)}) dx \quad (33)$$

$$- \frac{2}{n(n-1)} \sum_i \sum_{j \neq i} K_{x_i/b+1,b}^{\gamma}(\hat{\varepsilon}_j^{(v)}),$$

which yields the bandwidth $b^* = 0.0118$. See Hjort and Glad (1995) for details on (nearly) unbiased cross-validation. Further, we estimate the normalized density derivative $D(\varepsilon_t^{(v)})$ for $\varepsilon_t^{(v)} \in \{0, b^*, 2b^*\}$ as in (15) based on the modified gamma kernel. The corresponding results in Table 9 show that two out of three estimates are considerably negative, which indicates a possible pole situation and suggests the use of the standard gamma kernel. Figure

Table 9: Estimates of normalized density derivative for MEM errors based on intra-day trading volumes and realized kernel values. Estimates of the ratio $D(\varepsilon_t^{(m)}) := f'_\varepsilon(\varepsilon_t^{(m)})/f_\varepsilon(\varepsilon_t^{(m)})$, $m = v, rk$, based on the modified gamma kernel in the boundary region as in (15). $\varepsilon_t^{(m)}$ are errors from the MEM structure (31) fitted to deseasonalized nonzero 15-second trading volumes of Citigroup and realized kernel (RK) estimates for JP Morgan. b^* is LSCV bandwidth of the standard gamma kernel estimator: 0.0118 for trading volumes and 0.0206 for realized kernel estimates.

$\varepsilon_t^{(m)}$	Volume	RK
0	0.293	26.283
b^*	-10.100	59.915
$2b^*$	-14.399	53.235

9 displays estimates of the error density $f_\varepsilon(\varepsilon_t^{(v)})$ based on the standard and, for comparison, modified gamma kernel for the boundary region and a larger part of the support. While for both density estimates, the probability mass is quite concentrated close to the origin, the standard gamma kernel, being the method of choice, yields an estimate that lies clearly below the density implied by the modified kernel for the major part of the boundary region.

Finally, Figure 10 shows estimates of the conditional density of trading volumes for February 26 and 27, 2009, at 11am EST. On the latter day, Citigroup announced that the US treasury would be taking a major equity stake in the company, while the former day is included for comparison. As an alternative to the semiparametric approach, the plot also features the conditional density implied by maximum likelihood estimates of the MEM (31) assuming that the errors follow the widely-used gamma distribution (e.g. Engle and Gallo, 2006). The impact of the announcement on trading activity related to the Citigroup stock is clearly visible, as the conditional volume distribution for February 27 assigns considerably less weight to small transactions. The semiparametric density estimates and their parametric counterparts are quite close to each other in the interior of the support. The major difference occurs at the origin where the parametric densities exhibit a pole, which is not the case for the semiparametric estimates.

4.2. Forecasting Realized Volatility

Realized volatility measures computed from high-frequency data allow to construct more accurate estimates of the underlying lower frequency volatility (see, e.g., Andersen et al., 2010). We employ mid-quotes for JP Morgan

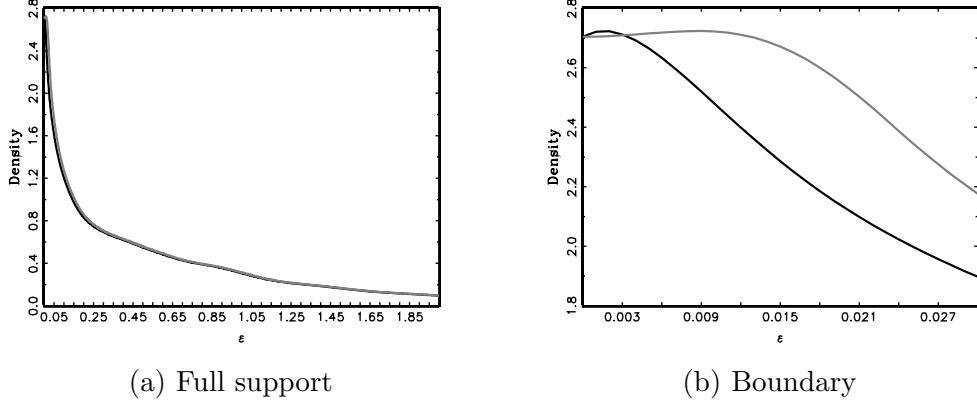


Figure 9: Estimates of MEM error density for intraday trading volumes (Citigroup). Estimates of the density $f_\varepsilon(\varepsilon_t^{(v)})$ from the MEM structure (31) fitted to deseasonalized nonzero 15-second trading volumes of Citigroup. Black solid line: standard gamma kernel. Grey solid line: modified gamma kernel. LSCV bandwidth of the standard gamma kernel, $b^* = 0.0118$, is used for both estimators.

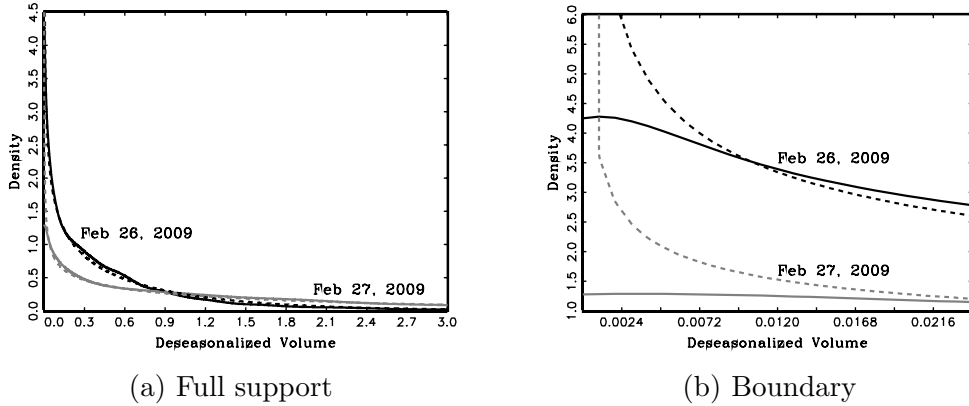


Figure 10: (Semi-)parametric conditional density of intraday volumes (Citigroup). Conditional densities at t given past information $\mathcal{F}_{t-1}^{(v)}$ based on the MEM structure (31) and the relationship (32). Parametric estimates (dashed lines) are implied by a ML approach assuming gamma distributed errors $\varepsilon_t^{(v)}$. Semiparametric estimates (solid lines) rely on QML estimates of $\mu_t^{(v)}$ and nonparametric estimates of $f_\varepsilon(x_t^{(v)}/\mu_t^{(v)})$ using the standard gamma kernel. Conditional densities are estimated for 11am EST on February 26 (black lines) and February 27, 2009 (grey lines).

from January 2006 to December 2009, which corresponds to 983 trading days, and clean the raw data as suggested in Barndorff-Nielsen et al. (2008b). The realized volatility for day t is simply defined as the sum of squared (mid-quote) returns $r_{i,t}$, $i = 1, \dots, N_t$. Barndorff-Nielsen and Shephard (2002) show that, in the absence of noise and with the number of intraday returns approaching infinity, this basic estimator is consistent for the latent integrated volatility, which under regularity conditions provides an unbiased measure of the conditional variance of (daily) returns. In practice, observed prices are contaminated by microstructure effects causing an inconsistency of the basic realized volatility estimator (e.g. Hansen and Lunde, 2006). Hence, we consider the noise-robust realized kernel estimator, which was proposed by Barndorff-Nielsen et al. (2008a) and takes the form

$$x_t^{(rk)} := \gamma_0 + \sum_{h=1}^H k\left(\frac{h-1}{H}\right) (\gamma_h + \gamma_{-h}), \quad \gamma_h := \sum_{i=1}^n r_{i,t} r_{i-h,t}, \quad (34)$$

where $k(\cdot)$ is the Parzen kernel and H the bandwidth. The number of returns used for the computation of the realized kernel, n , is lower than the total number of observations N_t due to the so-called jittering procedure. See Barndorff-Nielsen et al. (2008a) for details. Since (filtered) realized kernel estimates are used as inputs for kernel density estimators below, the two bandwidths involved have to be balanced in a way similar to Corradi et al. (2009), who propose nonparametric conditional density estimators for the integrated volatility. We ensure that their assumption A.1 is met by choosing H as in Section 4.3 of Barndorff-Nielsen et al. (2008a). To estimate the so-called noise-to-signal ratio, we follow Barndorff-Nielsen et al. (2008b).

Table 8 shows that the realized kernel estimates exhibit a similar persistence as trading volumes, which we account for by following Engle and Gallo (2006) and imposing a flexible MEM structure. Hence, we model the realized kernel value for day t , $x_t^{(rk)}$, analogously to (31), where the assumptions for the errors $\varepsilon_t^{(rk)}$ remain the same, while a slightly different specification is chosen for the conditional mean $\mu_t^{(rk)}$ (see AppendixA). We compute semi-parametric estimates of the conditional density $f_X(x_t^{(rk)} | \mathcal{F}_{t-1}^{(rk)})$ using the same approach as in Section 4.1, which in the given application, can be considered as a simple alternative to the fully nonparametric procedure proposed in Corradi et al. (2009). As Table 9 reports, the estimates of the normalized density derivative for the MEM errors are consistently positive, indicating that the

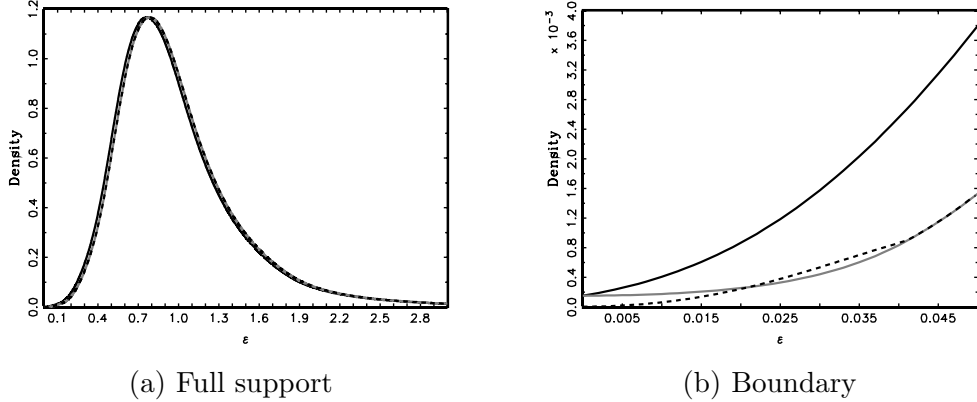


Figure 11: Estimates of MEM error density for realized kernel estimates (JP Morgan). Estimates of the density $f_\varepsilon(\varepsilon_t^{(rk)})$ from the MEM structure (31) fitted to realized kernel estimates for JP Morgan. Black solid line: standard gamma kernel. Grey solid line: modified gamma kernel. Black dashed line: refined modified gamma kernel v_1 . LSCV bandwidth of the standard gamma kernel, $b^* = 0.0206$, is used for all estimators.

corresponding density should be estimated using a modified gamma kernel. Thus, we first determine the optimal value of the constant c for the refined specification v_1 by minimizing the objective function (19). We compute the required pilot estimates of the unknown density and its first two derivatives as outlined in Section 2.3, which yields the threshold $c^* = 0.0863$.

Estimates of the MEM error density implied by all three types of gamma kernels considered are displayed in Figure 11 and indicate the following major results. First, as compared to the error density based on trading volumes in Figure 9, the mode of the distribution is further to the interior of the support. Second, the density exhibits a similar degree of right-skewness as was reported for the unconditional distribution of realized volatilities by Andersen et al. (2001). Finally, the density estimate based on the refined modified kernel tends to zero when approaching the boundary, instead of taking a strictly positive value at $\varepsilon_t^{(rk)} = 0$. This effect is caused by the low value of the threshold c^* , which pushes the shape parameter $\rho_b^{v_1}(\varepsilon_t^{(rk)})$ below one when smoothing at the boundary (see eq. (16)). A distribution of stock return volatility with vanishing probability mass close to the boundary is in line with financial theory, since stocks are “risky” assets for which investors demand a volatility premium (e.g. Merton, 1973).

Figure 12 displays conditional density estimates of realized kernel values

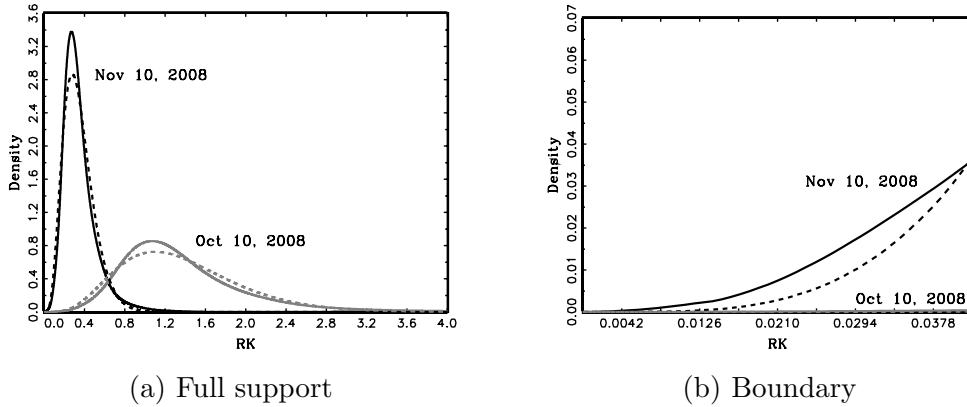


Figure 12: (Semi-)parametric conditional density of realized kernel estimates (JP Morgan). Conditional densities at t given past information $\mathcal{F}_{t-1}^{(rk)}$ based on the MEM structure (31) and the relationship (32). Parametric estimates (dashed lines) are implied by a ML approach assuming gamma distributed errors $\varepsilon_t^{(rk)}$. Semiparametric estimates (solid lines) rely on QML estimates of $\mu_t^{(rk)}$ and nonparametric estimates of $f_\varepsilon(x_t^{(rk)})/\mu_t^{(rk)}$ using the refined modified gamma kernel v_1 . Conditional densities are estimated for October 10 (grey lines) and November 10, 2008 (black lines). Realized kernel estimates are annualized.

for two days during the financial crisis 2007 – 2008: October 10, 2008, when the DJIA index fell by 8% at the start of the trading day, and November 10, 2008, when a major restructuring of the AIG bailout plan was announced. The density estimates are based on our semiparametric procedure using the refined modified gamma kernel and the parametric approach from Section 4.1. Except for some discrepancies around the mode and in the boundary region, the parametric estimates roughly match the semiparametric ones, indicating that the gamma distribution is a reasonable assumption for the MEM errors. With respect to dynamic changes, the conditional densities reflect the more unstable market environment on October 10, as the volatility distribution has its mode further away from the origin and is more dispersed. Further, as in case of the unconditional error density, the probability mass is vanishing close to the boundary for both days and estimators considered.

5. Conclusion

Gamma kernel estimators vary their shape according to the point of estimation along the support. For positive random variables, this location adaptiveness avoids the boundary bias associated with standard fixed kernel

estimators, while yielding strictly nonnegative density estimates by construction. We show for various density shapes that, in finite samples, the two original gamma kernel estimators outperform all boundary and boundary corrected fixed kernel type estimators at the boundary, in particular for settings with a large probability mass close to zero. For all other setups and in the interior of the support, their finite sample performance is comparable to the one of fixed-type boundary kernels. Moreover, with asymptotic considerations and finite sample illustrations we find that, for pole situations at zero, the two gamma kernel estimators differ substantially. In fact, the standard type is superior to the generally used modified version in this case. Therefore, we suggest a simple criterion to check for such situations. For all other settings, we propose a refined modified version of the gamma kernel estimator, which further improves upon the performance of the modified gamma kernel. Our technique is complemented by a data-driven way for choosing the specification parameters in the new refined gamma kernel. In two application settings, we demonstrate that, in particular in high-frequency finance, the suggested methodology yields superior results of practical impact.

Possible avenues for improving the performance of the proposed methods even further are manifold. First, nonparametric multiplicative bias correction techniques, as proposed in Hirukawa (2010), could be employed. Second, refined gamma kernel estimators could be combined with a local bandwidth variation in the spirit of Dai and Sperlich (2010). Finally, modifications similar to those suggested for gamma kernels could be developed for the Birnbaum-Saunders-type kernels put forward by Marchant et al. (2013).

Acknowledgements

For constructive comments and suggestions we thank the Co-Editor-in-Chief, Erricos John Kontoghiorghes, an anonymous Associate Editor and two anonymous referees, as well as the participants of the 2013 European Meeting of the Econometric Society and workshops at Humboldt-Universität zu Berlin. This research is supported by the Deutsche Forschungsgemeinschaft (DFG) via the Collaborative Research Center 649 "Economic Risk" and via the DFG grant SCHI-1127.

- Andersen, T. G., Bollerslev, T., Diebold, F. X., 2010. Parametric and non-parametric measurements of volatility. In: Ait-Sahalia, Y., Hansen, L. (Eds.), *Handbook of Financial Econometrics*. North Holland, Amsterdam, pp. 67–137.
- Andersen, T. G., Bollerslev, T., Diebold, F. X., Labys, P., 2001. The distribution of realized exchange rate volatility. *Journal of the American Statistical Association* 96 (453), 42–55.
- Barndorff-Nielsen, O., Hansen, P., Lunde, A., Shephard, N., 2008a. Designing realized kernels to measure the ex-post variation of equity prices in the presence of noise. *Econometrica* 76, 1481–1536.
- Barndorff-Nielsen, O., Hansen, P., Lunde, A., Shephard, N., 2008b. Realised kernels in practice: trades and quotes. *Econometrics Journal* 4, 1–32.
- Barndorff-Nielsen, O., Shephard, N., 2002. Econometric analysis of realized volatility and its use in estimating stochastic volatility models. *Journal of the Royal Statistical Society, Ser. B.* 64, 253–280.
- Bauwens, L., Giot, P., 2000. The logarithmic ACD model: an application to the bid-ask quote process of three NYSE stocks. *Annales D’Economie et de Statistique* 60, 117–149.
- Bouezmarni, T., Rombouts, J. V., 2010a. Nonparametric density estimation for multivariate bounded data. *Journal of Statistical Planning and Inference* 140 (1), 139 – 152.
- Bouezmarni, T., Rombouts, J. V., 2010b. Nonparametric density estimation for positive time series. *Computational Statistics & Data Analysis* 54 (2), 245 – 261.
- Bouezmarni, T., Scaillet, O., 2005. Consistency of asymmetric kernel density estimators and smoothed histograms with application to income data. *Econometric Theory* 21 (02), 390–412.
- Brownlees, C. T., Cipollini, F., Gallo, G. M., 2010. Intra-daily volume modeling and prediction for algorithmic trading. *Journal of Financial Econometrics* 8 (4), 1–30.

- Chen, S., 1999. Beta kernel estimators for density functions. *Computational Statistics & Data Analysis* 31 (2), 131–145.
- Chen, S., 2000. Probability density function estimation using gamma kernels. *Annals of the Institute of Statistical Mathematics* 52, 471–480.
- Corradi, V., Distaso, W., Swanson, N. R., 2009. Predictive density estimators for daily volatility based on the use of realized measures. *Journal of Econometrics* 150 (2), 119 – 138.
- Corsi, F., 2009. A simple approximate long-memory model of realized volatility. *Journal of Financial Econometrics*, 174–196.
- Dai, J., Sperlich, S., 2010. Simple and effective boundary correction for kernel densities and regression with an application to the world income and engel curve estimation. *Computational Statistics & Data Analysis* 54 (11), 2487 – 2497.
- Drost, F. C., Werker, B. J. M., 2004. Semiparametric duration models. *Journal of Business and Economic Statistics* 22, 40–50.
- Engle, R. F., 2002. New frontiers for ARCH models. *Journal of Applied Econometrics* 17, 425–446.
- Engle, R. F., Gallo, G. M., 2006. A multiple indicators model for volatility using intra-daily data. *Journal of Econometrics* 131 (1-2), 3–27.
- Fernandes, M., Grammig, J., 2005. Nonparametric specification tests for conditional duration models. *Journal of Econometrics* 127, 35–68.
- Ferraty, F., Quintela del Ro, A., Vieu, P., 2012. Specification test for conditional distribution with functional variables. *Econometric Theory* 28 (2), 363–386.
- Ferraty, F., Vieu, P., 2006. *Nonparametric functional data analysis: theory and practice*. Springer.
- Gasser, T., Müller, H., 1979. Kernel estimation of regression functions. In: Gasser, T., Rosenblatt, M. (Eds.), *Lecture Notes in Mathematics* 757. Springer, Heidelberg, pp. 23–68.

- Hagmann, M., Scaillet, O., 2007. Local multiplicative bias correction for asymmetric kernel density estimators. *Journal of Econometrics* 141, 213–249.
- Hansen, P. R., Lunde, A., 2006. Realized variance and market microstructure noise. *Journal of Business and Economic Statistics* 24 (2), 127–161.
- Hautsch, N., 2004. *Modelling Irregularly Spaced Financial Data: Theory and Practice of Dynamic Duration Models*. Springer, Berlin.
- Hautsch, N., Malec, P., Schienle, M., 2013. Capturing the zero: a new class of zero-augmented distributions and multiplicative error processes. *Journal of Financial Econometrics* forthcoming.
- Hirukawa, M., 2010. Nonparametric multiplicative bias correction for kernel-type density estimation on the unit interval. *Computational Statistics & Data Analysis* 54 (2), 473 – 495.
- Hjort, N. L., Glad, I. K., 1995. Nonparametric density estimation with a parametric start. *The Annals of Statistics* 23, 882–904.
- Jones, M., 1993. Simple boundary correction for kernel density estimation. *Statistics and Computing* 3, 135–146.
- Jones, M. C., Foster, P. J., 1996. A simple nonnegative boundary correction method for kernel density estimation. *Statistica Sinica* 6, 1005–1013.
- Karunamuni, R. J., Albers, T., 2005. On boundary correction in kernel density estimation. *Statistical Methodology* 2, 191–212.
- Lancaster, T., 1997. *The Econometric Analysis of Transition Data*. Cambridge University Press, Cambridge.
- Marchant, C., Bertin, K., Leiva, V., Saulo, H., 2013. Generalized birnbaum-saunders kernel density estimators and an analysis of financial data. *Computational Statistics & Data Analysis* 63 (0), 1 – 15.
- Marron, J. S., Ruppert, D., 1994. Transformations to reduce boundary bias in kernel density estimation. *Journal of the Royal Statistical Society. Series B* 56 (4), 653–671.

- Merton, R., 1973. An intertemporal capital asset pricing model. *Econometrica* 41, 867 – 888.
- Michels, P., 1992. Asymmetric kernel functions in non-parametric regression analysis and prediction. *Journal of the Royal Statistical Society. Series D (The Statistician)* 41, 439–454.
- Quintela del Ro, A., Ferraty, F., Vieu, P., 2011. Analysis of time of occurrence of earthquakes: a functional data approach. *Mathematical Geosciences* 43 (6), 695–719.
- Robinson, P., Henry, M., 2003. Higher-order kernel semiparametric m-estimation of long memory. *Journal of Econometrics* 114 (1), 1–27.
- Scaillet, O., 2004. Density estimation using inverse and reciprocal inverse gaussian kernels. *Journal of Nonparametric Statistics* 16, 217–226.
- Schuster, E., 1958. Incorporating support constraints into nonparametric estimators of densities. *Communications in Statistics, Part A - Theory and Methods* 14, 1123–1136.
- Zhang, S., 2010. A note on the performance of gamma kernel estimators at the boundary. *Statistics and Probability Letters* 80, 548–557.

AppendixA. MEM Specifications

For trading volumes, we specify the conditional mean $\mu_t^{(v)}$ in (31) using the logarithmic MEM proposed by Bauwens and Giot (2000). The latter does not require parameter constraints to ensure the positivity of $\mu_t^{(v)}$ and implies

$$\ln \mu_t^{(v)} = \omega + \sum_{i=1}^p \alpha_i \ln x_{t-i}^{(v)} + \sum_{i=1}^q \beta_i \ln \mu_{t-i}^{(v)}, \quad (\text{A.1})$$

where the lag structure is chosen according to the Schwartz information criterion (SIC).

In case of volatilities, we consider (A.1) with $p = 1$, but augmented by the lags of (logarithmic) weekly and monthly realized kernel estimates, which

are defined as the averages

$$x_{t,w}^{(rk)} =: \frac{1}{5} \sum_{j=0}^4 x_{t-j}^{(rk)} \quad \text{and} \quad x_{t,m}^{(rk)} =: \frac{1}{20} \sum_{j=0}^{19} x_{t-j}^{(rk)}. \quad (\text{A.2})$$

This extension is motivated by the widely-used heterogeneous autoregressive (HAR) model for realized volatilities proposed by Corsi (2009) and yields

$$\ln \mu_t^{(rk)} = \omega + \alpha^d \ln x_{t-1}^{(rk)} + \alpha^w \ln x_{t-1,w}^{(rk)} + \alpha^m \ln x_{t-1,m}^{(rk)} + \sum_{i=1}^q \beta_i \ln \mu_{t-i}^{(rk)}, \quad (\text{A.3})$$

where q is determined using the SIC.